

# New scaffolds for O-GlcNAc transferase inhibition, by hit and synthetic route optimisation

Kevin van Eekelen<sup>a</sup>, Elena M. Loi<sup>a,b</sup>, Cyril Balsollier<sup>a,b</sup>, Roland J. Pieters<sup>a</sup>

<sup>a</sup> Department of Chemical Biology & Drug Discovery, Utrecht Institute for Pharmaceutical Sciences, Utrecht University, 3584 CG Utrecht, The Netherlands

<sup>b</sup> Department of Pharmaceutical Chemistry, Faculty of Pharmacy, University of Ljubljana, Ljubljana, 1000, Slovenia

[k.vaneekelen@students.uu.nl](mailto:k.vaneekelen@students.uu.nl)

## Abstract

Perturbations in O-GlcNAcylation, modulated by O-GlcNAc transferase (OGT) and O-GlcNAcase, have been observed in diabetes, cancer, cardiovascular disease, and Alzheimer's disease. Therefore, OGT is an interesting therapeutic target for the medical community. Current potent OGT inhibitors usually lack target specificity, e.g., BZX2 and OSMI-1, or cell-permeability e.g. OSMI-4. To explore novel OGT inhibitors, hit optimisation was performed on the recently identified compound **Vs-51**, creating a small library. In total, five promising derivatives of **Vs-51** were synthesised, of which the most potent one inhibited the enzyme with an  $IC_{50}$  of  $27 \pm 13 \mu\text{M}$ . Furthermore, the derivatives provided improved insight into potential **Vs-51** enhancements. For the second part of this study, a DNA encoded library was used to find new scaffolds for OGT, leading to two promising hits. A new synthetic pathway was established for one of these hits (**10115**) while allowing easy derivatisation options. The ease of tunability of the provided scaffold through the here described synthesis route offers a potential new series of potent OGT inhibitors.

**Keywords:** O-GlcNAcylation; OGT inhibitors; Virtual screening; Hit optimisation; DNA encoded library; Organic synthesis.

## 1. Introduction

O-GlcNAcylation is a dynamic posttranslational modification that attaches and detaches a  $\beta$ -N-acetyl-D-glucosamine (O-GlcNAc) moiety to serine (Ser) and threonine (Thr) residues of intracellular proteins. O-GlcNAcylation modifies a protein's function, stability and interactions; therefore, it plays a critical role in biological processes [1,2]. O-GlcNAcylation is modulated by a pair of enzymes: O-GlcNAc transferase (OGT) and O-GlcNAcase (OGA). OGT regulates the addition of the GlcNAc moiety

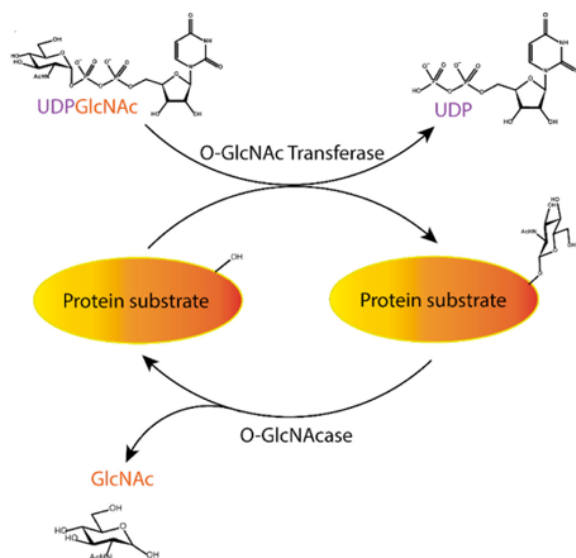


Figure 1: O-GlcNAcylation process

onto the Ser and Thr residues from uridine diphosphate N-acetylglucosamine (UDP-GlcNAc), and OGA removes the GlcNAc moiety, Figure 1 [3,4]. Dysfunctions in the O-GlcNAcylation process are involved in multiple human diseases since perturbations in O-GlcNAcylation have been observed in diabetes, cancer, cardiovascular disease, and Alzheimer's disease [3,5–7]. This makes OGA and OGT interesting therapeutic targets for the medical community. While OGA inhibitors, like MK-8719, have already moved into phase 1 clinical trials, OGT inhibitors still have a long way to go [8]. OGT is a more complex and challenging target because the instability of the enzyme makes it hard to assess inhibitor function. Even though OGT activity has been studied extensively and can be altered in *in vitro* and *in vivo* disease models, there are still unanswered questions about the exact role of OGT in related pathogenic processes [9–12].

The structure of the OGT enzyme consists of two principal regions: the N-terminal tetratricopeptide (TPR) region and the C-terminal catalytic region. The TPR region contains a highly conserved asparagine ladder that runs throughout the region and is involved in protein-protein interactions and protein acceptor binding [13,14]. The C-terminal catalytic region is divided into three subdomains, consisting of two catalytic domains (Cat-1 and Cat-2) that form an active site pocket for substrate binding. The third domain is an intervening domain, which couples the two catalytic domains and is packed against the outer face of the Cat-2 domain [15]. It has been shown that UDP-GlcNAc first binds in a pocket formed between the two catalytic domains

[15]. Then, the bound UDP-GlcNAc is activated through interactions between the side chain of Thr-921 and the amide backbone of the N-terminus of the  $\alpha$ -helix and Lys-842 and one oxygen of the  $\beta$ -phosphate [15]. The current knowledge of the OGT active site combined with the 3D structure allows researchers to design novel inhibitors for OGT using docking studies since potent and specific OGT inhibitors could also play a vital role in the target validation process.

Small molecule inhibitors of OGT have therefore been gaining interest. Several of these OGT inhibitors have already been used to study the role of OGT both in pathogenic processes and in several fundamental cellular pathways. Early OGT studies used inhibitors that were non-specific but were able to permeate the cells, such as alloxan, Figure 2 [16].

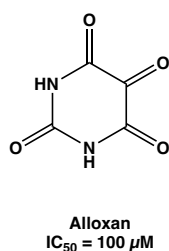


**Figure 2:** Alloxan, a small molecule inhibitor for OGT.

Alloxan lacked specificity and potency and therefore required high concentrations for cellular work. Most natural donor substrate (O-GlcNAc) mimic inhibitors have been discontinued due to a lack of cell permeability. However, inhibitors such as Ac<sub>4</sub>-5S-GlcNAc exploit the cell's metabolic conversion machinery and get converted to UDP-5S-N-acetylglucosamine to form a potent OGT inhibitor, Figure 3. Unfortunately, UDP-5S-N-acetylglucosamine lacks target specificity and solubility, complicating data interpretation of *in vivo* assays and use as a therapeutic drug [17].

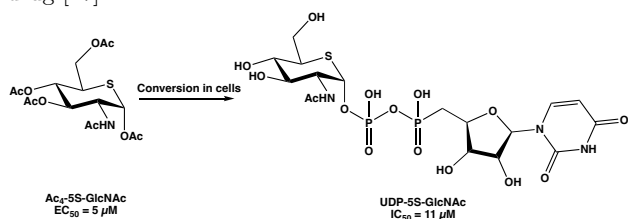


**Figure 3:** Ac<sub>4</sub>-5S-GlcNAc is converted to the potent inhibitor UDP-5S-GlcNAc

Lately, the focus has therefore been shifted to prepare cell-permeable inhibitors with an improved target specificity and potency, made possible by new insights obtained from the 3D structure of OGTs active site. This, in combination with a technique called high-throughput screening (HTS), led to the discovery of both reversible and irreversible novel nanomolar inhibitors for OGT [1]. One of the most potent OGT inhibitors from such screening is a benzoxazolinone-core containing compound named BZX2, Figure 4A. BZX2 is a cell-permeable, irreversible covalent OGT inhibitor, consisting of a five heteroatom dicarbamate moiety with an acetyl substituent on the BZX core and an electron-donating p-methoxy substituent on the phenyl group. BZX2 is a potent inhibitor with an  $IC_{50} < 10 \mu M$  but shows many off-target effects [18,19].

The best scaffolds to date are quinolinone-6-sulfonamide (Q6S) based compounds. The Q6S moiety has proven to be a good uridine mimic, both in HTS and validation assays. In the interaction with the OGT binding pocket, the His-901 interacts with the quinolinone ring through direct stacking. Additionally, the carbonyl and the adjacent nitrogen in the heterocycle interact with Arg-904 and Ala-896 like the N in position 3 and O in position 4 of uracil. Furthermore, a hydrogen bond is formed between Lys-898 and the sulphonamide oxygen of the Q6S moiety, mimicking the interactions of the ribose hydroxyls in O-GlcNAcylation. These observations led to the design of various Q6S-based inhibitors named the OSMI derivatives [20]. The structures of these OSMI compounds are U-shaped, improving their ability to inhibit OGT. The U-shape allows the inhibitors to fully occupy the space that both the peptide segment and the uridine usually accommodate. However, the quinolinone moiety is more crucial for the target affinity [20]. The first OSMI compound designed is named OSMI-1. It had a relatively high  $K_d$  of  $\pm 140$  nM and showed off-target effects. The OSMI-1 compound was therefore optimised by installing a chlorine in the 7 position of the quinolinone part of the molecule, making OSMI-4. This allowed the new compounds to make a cation-dipole interaction in the binding pocket. The OSMI-4 compounds showed reduced off-target effects while providing binding affinity in the low nanomolar range ( $K_d = 8$  nM for OSMI-4a). Initially, it was thought that OSMI-4b would be converted to OSMI-4a during cell permeation. Still, recent publications showed that the ester form could stay intact and even provided a higher target affinity than the free acid form,  $IC_{50} = 0,5 \pm 0,5 \mu M$  over  $IC_{50} = 1,5 \pm 0,6 \mu M$  respectively [20,21]. Unfortunately, the  $EC_{50} = 3 \mu M$  for OSMI 4 shows that the OSMI compounds lack cell permeability, maintaining the strong need for new ways to find and design new scaffolds.

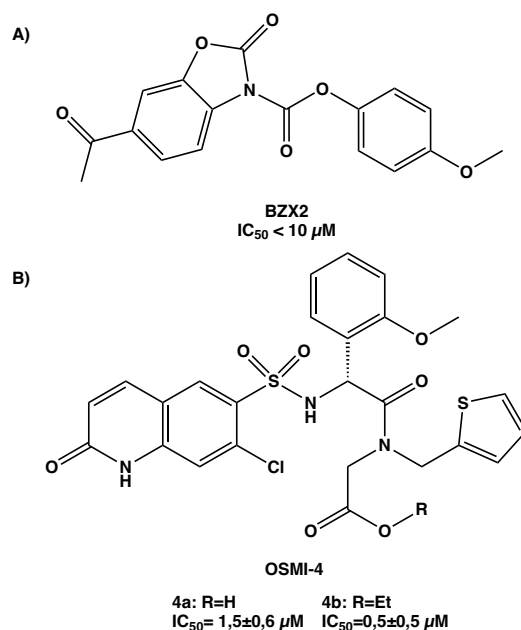


**Figure 4:** A) BZX2, a potent cell-permeable, covalent OGT inhibitor B) OSMI-4, the best OGT inhibitor up to date.

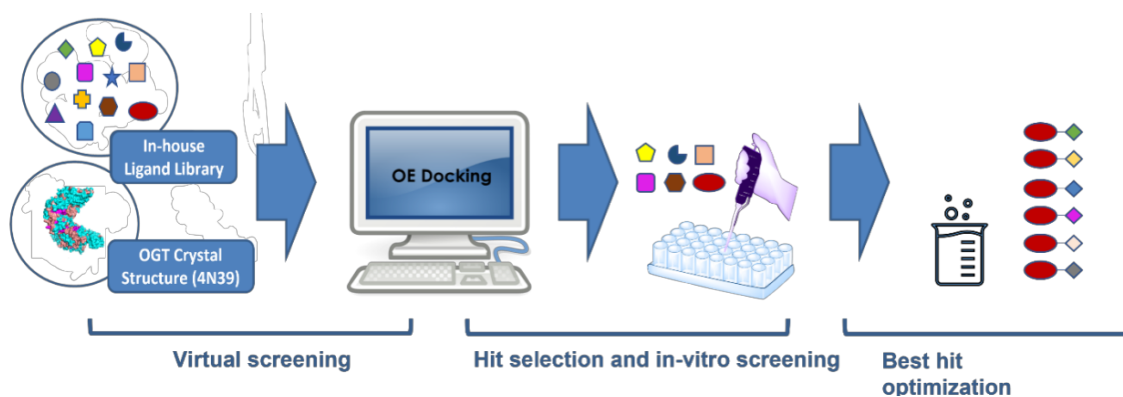


Figure 5: A schematic overview of the study that found Vs-51.

## 2. Virtual screening

Virtual screening is a computational method in drug discovery that aims to discover new possible binders for a specific target among libraries of small molecules. This is done by applying knowledge about the protein target or bioactive ligands and searching for similarity, substructure searching, pharmacophore-based searching and 3D shape matching. All these tests are performed against a selected crystal structure of the protein target. Since this approach is highly dependent on the quality and quantity of available data, correct information is crucial. In virtual screening, the 3D structure of the candidate molecules is docked in the biological target protein or receptor; these are then ranked based on their predicted binding affinity [22].

In a study to design novel OGT inhibitors, a process that combined virtual screening, hit selection, and hit optimisation was conducted, Figure 5. For the virtual screening campaign, an in-house library of more than two million compounds was used, out of which all possessed drug-like properties and were commercially available. In O-GlcNAcylation, a double hydrogen bond is formed between the uridine moiety of UDP and Ala-896 of OGT; furthermore, it was shown that the OSMI compounds also utilise this interaction in binding to OGT. Therefore, the docking experiment was conducted with a constraint to mimic this hydrogen bond interaction [12,15,23]. The 120 most promising hits were selected and further analysed. Clusters were made for similar chemotypes of these molecules, resulting in nine families. Eighteen molecules were chosen, purchased, and tested from these clusters based on the predicted binding poses and their synthetic accessibility and chemical diversity. Out of these compounds, a molecule named Vs-51 showed to be the most promising, having an  $IC_{50}$  of 7  $\mu$ M and was therefore selected to be further optimised (Figure 6A). The FRED and Hybrid tools from Openeye were used as guidance in designing a new library based on this compound. After further analysis of the interaction between Vs-51 and OGT, it was found that the triazole is anchoring the inhibitor in the same region as UDP-GlcNAc, mimicking a critical interaction between phosphate groups of UDP-GlcNAc and the present nucleotides. Therefore, it was decided to retain this part and modify the substituents to investigate and optimise the structure-activity relationships and improve physicochemical properties. Since it was shown that in OSMI-4, a cation-dipole interaction was formed between

Lys-898 and the chlorine on the Q6S moiety, the substituent in the six position of the indolinone ring was also changed to try and mimic this interaction [12,20].

In the first part of this research, multiple novel OGT inhibitors were found and synthesised using hit optimisation. To improve target affinity, five derivatives of Vs-51 were made by changing the triazole and the indolinone ring substituents, as shown in Figure 6B. The FRED and Hybrid tools from Openeye showed that elongating the R<sub>1</sub> and R<sub>2</sub> substituents of the triazole would allow compounds to further reach into the active site and obtain higher affinities by increasing the number of interactions in the pocket (Figure S1). Subsequently, the difference between the piperazine and the morpholine derivatives will showcase if a charge improves cell permeability and target affinity. The addition of the chlorine in the R<sub>3</sub> position on the indolinone ring is

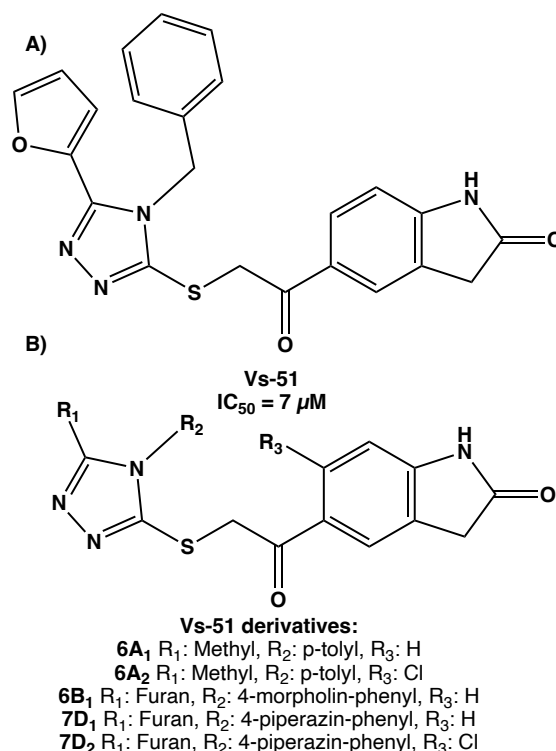
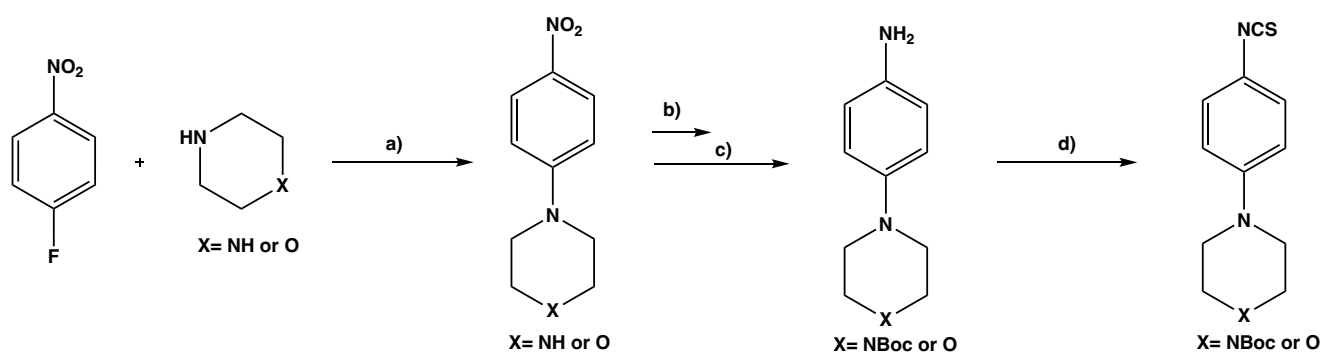


Figure 6: A) The structure of Vs-51 B) The overview of the five derivatives from this research.



**Scheme 1:** Reactions to form the isothiocyanates: a)  $\text{Et}_3\text{N}$ , MeCN,  $80^\circ\text{C}$  b)  $\text{Boc}_2\text{O}$ ,  $\text{H}_2\text{O}$  c)  $\text{H}_2$ , 5% Pd/C, EtOH d)  $\text{CS}_2$ ,  $\text{Et}_3\text{N}$ ,  $\text{TsCl}$ , THF.

introduced to see the effect of a cation-dipole interaction on target affinity.

### 3. Hit optimisation of Vs-51

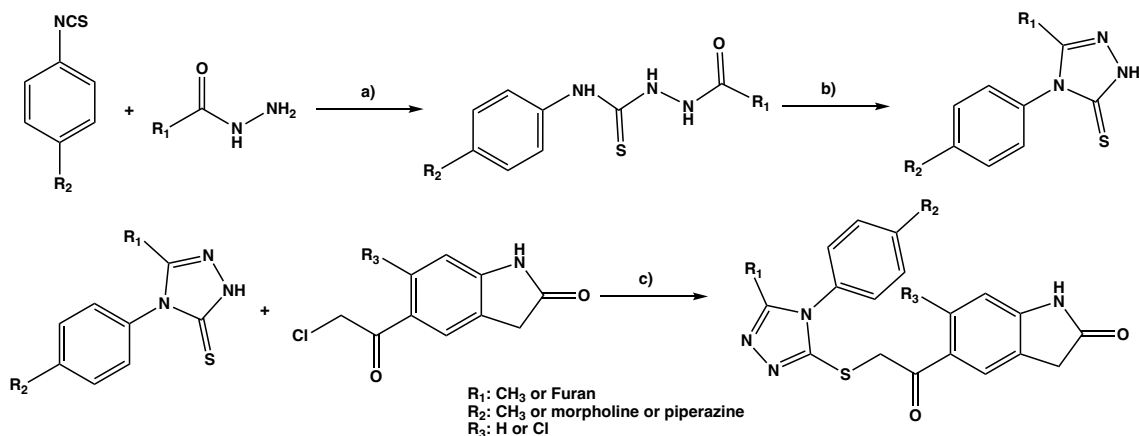
Scheme 1 illustrates how the 4-morpholino-phenyl and 4-piperazino-phenyl isothiocyanates were synthesised from in-house chemicals. First, a nucleophilic aromatic substitution was performed by refluxing 1-fluoro-4-nitrobenzene and either piperazine or morpholine in the presence of triethylamine. Subsequently, the piperazine derivative was protected using a *tert*-butyl carbamate group. Next, the nitro groups for both products were reduced to amines using 5 wt.% palladium on charcoal and hydrogen gas. Then the resulting anilines were reacted with carbon disulphide and triethylamine at room temperature to form a dithiocarbamate salt, which was decomposed to an isothiocyanate group using tosyl chloride.

To finalise the derivatives of **Vs-51**, first, the 1,2,4-triazole-3-thiol was synthesised by refluxing the isothiocyanate and hydrazide compounds to form the thiourea intermediate, followed by reflux under alkaline conditions to do a cyclisation. Then a nucleophilic substitution with the indolinone scaffold led to the final derivatives, scheme 2.

The hit optimisation of compound **Vs-51** was conducted to improve insight into the compound's binding mode in OGT. By introducing the modifications in position  $\text{R}_1$  on the triazole, it was found that the presence of a furan ring improves binding. This was concluded by comparing compound data with others from earlier hit optimisation studies of compound **Vs-51** [12]. It is thought that this is because the furan provides a better fit into the pocket close

to the sugar-binding region. Therefore, a furan substituent in  $\text{R}_1$  will be used for further hit optimisation studies. Next, it was hypothesised that introducing a *p*-tolyl in the  $\text{R}_2$  position of the triazole would increase the rigidity of the molecule and, according to the docking, should fit in the hydrophobic part of the binding site. Unfortunately, when compared to a compound with just a phenyl in  $\text{R}_2$  from earlier data, it was found that replacing the phenyl with toluene led to a decrease in inhibitory activity. According to the docking studies performed, elongating the molecule in position  $\text{R}_2$  would allow reaching further into a wider area of the active site. Hence, morpholine and piperazine rings were introduced on top of the phenyl, aiming to improve water solubility and, therefore, cell-permeability of the inhibitors [12]. However, the modification of the morpholine ring led to a complete loss of activity, probably due to steric hindrance, which prevents the molecule from fitting into the OGT active site. As for the piperazine derivatives' binding affinity remains unknown since these compounds are yet to be tested. However, looking at the results obtained from the morpholine derivatives, these compounds are also expected to lose activity due to steric hindrance.

Furthermore, the  $\text{R}_3$  position of the indolinone part of the compound in this hit optimisation study was changed. A chlorine atom was introduced to mimic a cation-dipole interaction seen in OSMI-4. This change made the compounds synthesised in this research insoluble, making them unable to be tested in the fluorescence assay. In other derivatives it was found that the chlorine reduced target affinity [12]. It has been seen in docking images that the introduction of the chlorine atom changes the position of

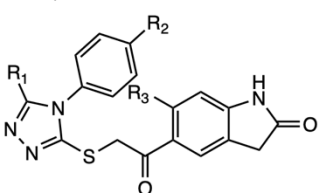


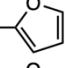
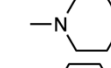
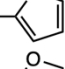
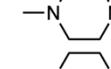
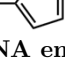
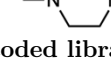
**Scheme 2:** Synthesis of final derivatives; a) EtOH, Reflux b) 2M 50% EtOH, Reflux c)  $\text{K}_2\text{CO}_3$ , EtOH,  $40^\circ\text{C}$ .

the indolinone part in the active site, Figure S1. This is probably due to the size of the chlorine atom and might be the reason that the inhibitory effect is reduced. It would be interesting to test the effect of a fluorine atom in future research since this is a smaller atom and can also undergo cation dipole interactions. An overview of all the synthesised derivatives and the corresponding  $IC_{50}$  values determined using the fluorescence assay are given in Table 1 [12].

**Vs-51** has shown to be a suitable scaffold for OGT inhibitors with an  $IC_{50}$  of  $7\mu\text{M}$ . However, **Vs-51** shows off-target effects in AMO1 cells, limiting therapeutic use. Therefore, the results obtained in this research should be used as a starting point in the FRED and Hydrid tools of Openeye to explore further improvements.

**Table 1:** Overview of **Vs-51** derivatives and inhibitory activity.



Name	R <sub>1</sub>	R <sub>2</sub>	R <sub>3</sub>	$IC_{50}$ ( $\mu\text{M}$ ) $\pm$ SD
6A <sub>1</sub>	—CH <sub>3</sub>	—CH <sub>3</sub>	—H	$27 \pm 13$
6A <sub>2</sub>	—CH <sub>3</sub>	—CH <sub>3</sub>	—Cl	Not soluble
6B <sub>1</sub>			—H	No inhibition
7D <sub>1</sub>			—H	To be tested
7D <sub>2</sub>			—Cl	To be tested

#### 4. DNA encoded library

A second way to find new inhibitors is by using a DNA encoded library (DEL). DEL is a method that allows the screening of millions of chemical compounds in a single experiment. The DEL libraries are first produced by attaching DNA strands to all the fragments they possess, that code for how the corresponding component was made. Then proteins are used to couple all the different strands within a library so that all the compounds can be used for affinity testing simultaneously. After affinity testing on the target protein, analysis can determine which structures showed binding interactions with the substrate. Subsequently, the most promising structures can be selected and synthesised to validate the binding assays.

One company that utilises this technique is WuXi AppTec using the program DELOpen [24]. DELOpen gives free

access to 27 libraries containing over 4,2 billion compounds for academic use, allowing users to conduct affinity selection experiments in their labs. Then, the samples are sent to WuXi AppTec, and they take care of post-selection processing, sequencing, and data analysis, possibly leading to high-affinity inhibitors. These are then synthesised by WuXi AppTec and used in binding assays to validate the hits, as shown in Figure 8 [24]. Since this is a free process, this all happens blinded to the customer. Once promising hits are identified by WuXi AppTec and validated by the customer, they can decide to disclose the target in exchange for the chemical structures.

DELOpen has been used in this study to provide promising novel OGT inhibitors. Four sub-libraries came back as interesting in the screening, providing six different compounds, of which two came back as hits. These hits are named **10115** and **10207**, respectively inhibiting with an  $IC_{50}$  =  $24\mu\text{M}$  and  $67\mu\text{M}$ , Figure 7. New libraries can be created by changing substituents to improve these compounds' binding affinities and cell permeability.

This study will mainly focus on developing a robust synthetic route that allows the synthesis of **10115** and its derivatives to validate the inhibition of OGT and create a small library. Compound **10115** and four derivatives were synthesised, with changes in the R<sub>1</sub> and R<sub>2</sub> positions on the phenyls to determine what drives improved target affinity, Figure 9. At last, the R<sub>3</sub> substituent of the carbonyl was

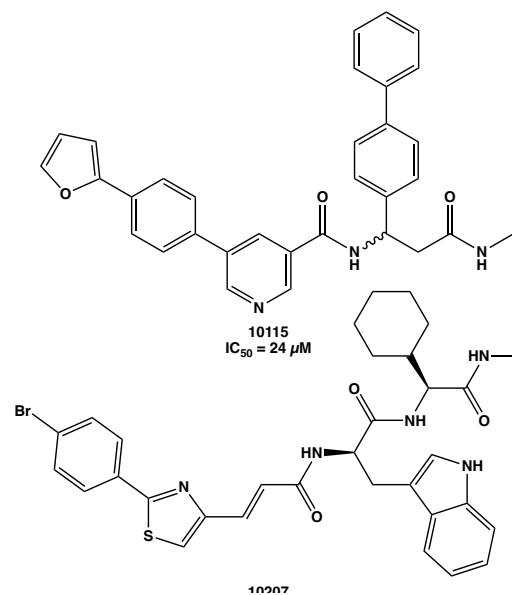
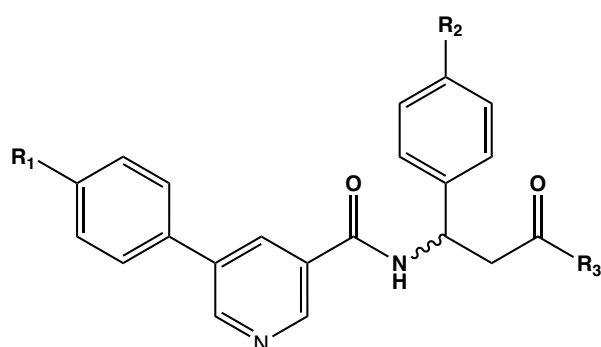


**Figure 7:** The two hits the DEL provided, **10115** and **10207**, and their  $IC_{50}$  values.



**Figure 8:** Schematic overview of the DELOpen process at WuXi AppTec.

modified to see the effect of a charge on cell permeability and target affinity. Combined, all these derivatives will form a new family of novel OGT inhibitors. Also, hit optimisation studies will improve insight into how OGT inhibitors from these clusters can be enhanced in physicochemical properties and have an increased target affinity and cell permeability.



**10115 derivatives:**

**5H** R<sub>1</sub>: Furan, R<sub>2</sub>: Br, R<sub>3</sub>: Et

**5G** R<sub>1</sub>: Br, R<sub>2</sub>: Phenyl, R<sub>3</sub>: Et

**6G** R<sub>1</sub>: Furan, R<sub>2</sub>: Phenyl, R<sub>3</sub>: OEt

**6G-A** R<sub>1</sub>: Furan, R<sub>2</sub>: Phenyl, R<sub>3</sub>: OH

**10115** R<sub>1</sub>: Furan, R<sub>2</sub>: Phenyl, R<sub>3</sub>: NHMe

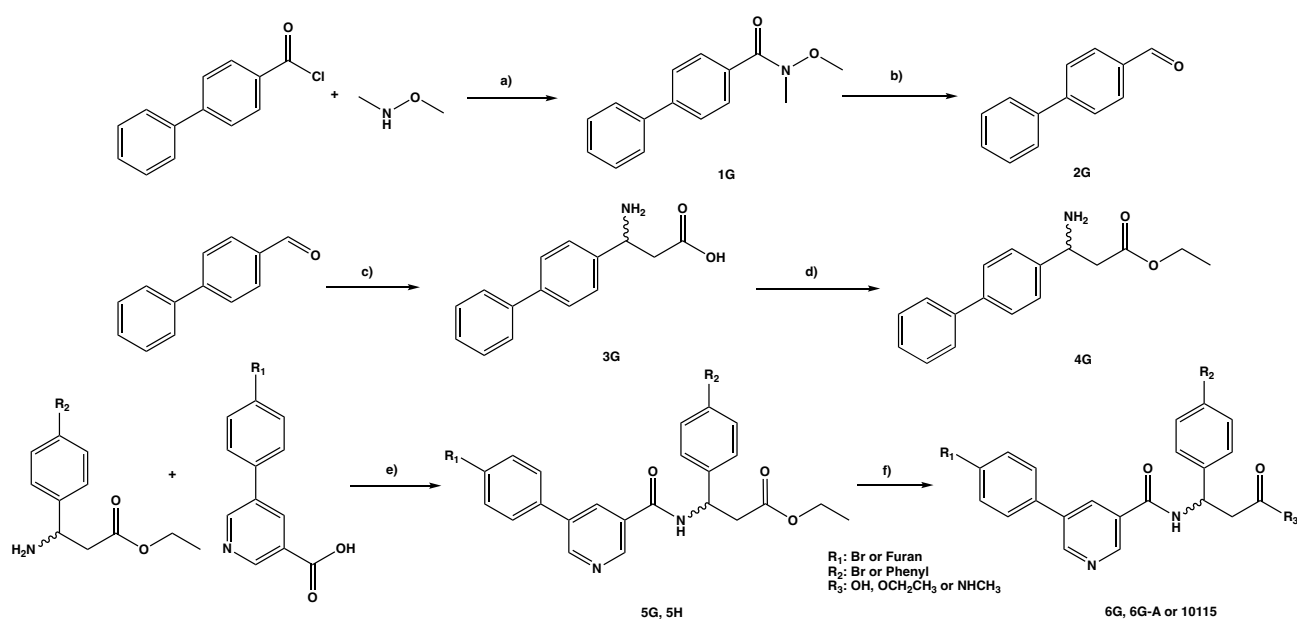
**Figure 9:** Overview of the derivatives of **10115** that will be synthesised in this research.

### 5. Design of a synthetic route for 10115

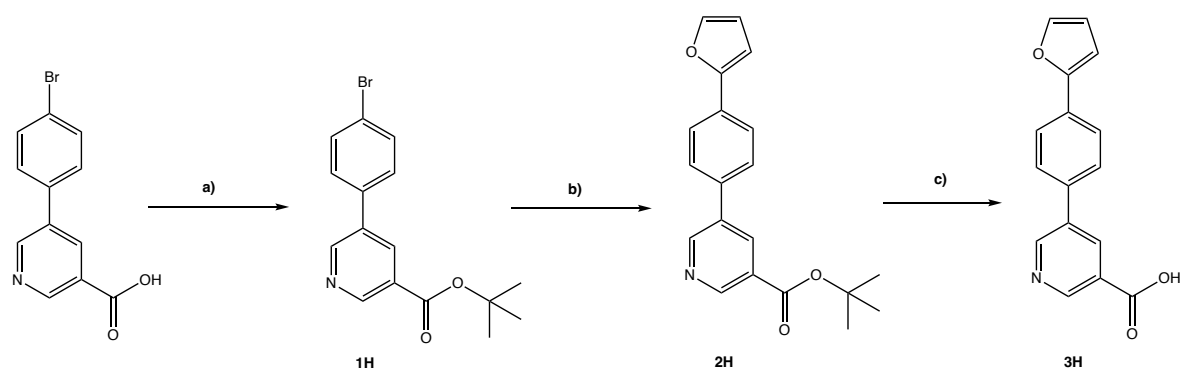
The second aim of this project was to design a synthesis route for 10115 and its derivatives. Initially, it was thought that this could be achieved by a Suzuki coupling between phenylboronic acid and ethyl 3-amino-3-(4-bromophenyl) propanoate, followed by a peptide coupling with 5-(4-bromophenyl) nicotinic acid. This product would then undergo a Suzuki coupling with furan-2-boronic acid and, at last, amination of the ethyl ester to form **10115**. Unfortunately, after trying over 12 different reaction conditions in the first step, the Suzuki coupling never

worked. Within these 12 attempts, the base, catalyst, solvent system, and additives (i.e. KF) were altered to improve the stability of the boronic acid since homocoupling was often observed. In this study, three additional improvements were tried. The first was the use of phenylboronic acid pinacol ester to improve the stability of the boronic acid. In a second attempt, the boronic acid was installed on ethyl 3-amino-3-(4-bromophenyl) propanoate, and then bromophenyl was used in a Suzuki coupling. A Kumada coupling was tried in a third attempt to make this coupling work; this cross-coupling reaction uses a Pd or Ni catalyst, a Grignard reagent, and an aryl halide. Unfortunately, all three approaches did not yield the desired product. Therefore, it was decided to do retrosynthesis of **10115** and design a new synthesis route that could be done from in-house chemicals. Since the synthesis of the biphenyl showed to be unsuccessful, the aim was to avoid a cross-coupling reaction on the bromophenyl part. This resulted in the synthesis scheme which is shown in Scheme 3.

This approach started with a reaction between an acid chloride and *N,O*-dimethyl hydroxylamine, which is a Weinreb reagent. Usually, the direct transformation of carboxylic acids, esters and acid chlorides to aldehydes or ketones do not give high yields due to the high reactivity of the ketone intermediates. To overcome these issues, Weinreb reagents are used in organic chemistry to form stable intermediates and, therefore, aldehydes and ketones. Within this project, the Weinreb intermediate (**1G**) was reacted with LiAlH<sub>4</sub> to reduce it to the corresponding aldehyde (**2G**) in a high yield [25]. Next, a Rodionov reaction on the aldehyde yielded the β-amino acid, **3G** [26]. This reaction, however, gave a relatively low yield (35%) for the biphenyl compound, which is in line with the literature on this exact reaction [27]. Therefore, further optimisation is crucial when used on a larger scale in the future. This



**Scheme 3:** Synthesis overview to **10115** and its derivatives; a) Et<sub>3</sub>N, DCM b) LiAlH<sub>4</sub>, THF c) Malonic acid, NH<sub>4</sub>OAc, EtOH, Reflux d) SOCl<sub>2</sub>, EtOH, Reflux e) HATU/DIPEA, DMF f) 2M NaOH, EtOH, Reflux or 40% MeNH<sub>2</sub>, MeOH



**Scheme 4:** Synthesis scheme of **3H**; a)  $\text{Boc}_2\text{O}$ , DMAP, THF, Reflux b) Furan-2-boronic acid,  $\text{Pd}(\text{dppf})\text{Cl}_2$ ,  $\text{NaOtBu}$ , 20%  $\text{H}_2\text{O}$  in THF, Reflux c) TFA, DCM.

should be possible since a recent article by Rodríguez-Mata et al. showed that changing the molar equivalents between the reactants could achieve an 84% yield in this reaction [28]. In the next step, esterification on the carboxylic acid was done using thionyl chloride to form an acid chloride intermediate to increase the electrophilicity of the carbonyl. To then undergo esterification with ethanol to yield **4G**. To form the next product, **4G** should be reacted with 5-(4-(furan-2-yl)phenyl)nicotinic acid (**3H**), which was first made from 5-(4-bromophenyl) nicotinic acid, Scheme 4.

**3H** was synthesised as a separate fragment since it allowed multiple derivatives synthesised with just a peptide coupling as the final reaction, easing purification. To synthesise **3H**, first, the 5-(4-bromophenyl) nicotinic acid was protected using DMAP and Di-*tert*-butyl dicarbonate to yield **1H**. Then a Suzuki coupling with furan-2-boronic acid was done using  $\text{Pd}(\text{dppf})\text{Cl}_2$  and sodium *tert*-butoxide in 20% water/THF to yield **2H**. In the final step, **2H** was deprotected using TFA to yield **3H**.

Then the final compounds could be synthesised by doing a peptide coupling using HATU/DIPEA in DMF. As shown in the lower part of scheme 3, this was done between four different fragments to yield three ester derivatives of **10115**. These derivatives are esters in  $\text{R}_3$  and have either an extension with a furan ring in  $\text{R}_1$  (**5H**), or a phenyl in  $\text{R}_2$  (**5G**) or both to give **6G**. From derivative **6G**, **10115** could be synthesised by amination with 40% methylamine in methanol. The last derivative was synthesised by hydrolysis of **6G**, yielding the corresponding carboxylic acid (**6G-A**).

This approach allowed us to synthesise compound **10115** and its four derivatives, which form the start of a small library. With the ethyl ester in  $\text{R}_3$  and the bromines in the  $\text{R}_1$  and  $\text{R}_2$  positions of the fragments, a lot of different substituents can be made to expand the library and gain more knowledge on OGT inhibition. One of the downsides of this approach is that it does not allow for the stereoselective synthesis of the final compounds. The starting material (ethyl 3-amino-3-(4-bromophenyl) propanoate) from the original synthesis route could be obtained enantiomerically pure from chemical suppliers. Therefore, it allowed for the synthesis of the R and S isomers, while this approach only allows the racemic mixture to be synthesised. The enantiomers are crucial since the 3D structures of the inhibitors differ significantly. Thus, they are expected to have different  $\text{IC}_{50}$  values since the

biphenyl part would point towards a different pocket in OGT. Therefore, separating the enantiomers and finding the most active is essential, especially considering that the previously determined  $\text{IC}_{50}$  of 24  $\mu\text{M}$  of **10115** is also derived from the racemic mixture. For that reason, it is thought that the more active enantiomer can potentially be as potent as the most potent OGT inhibitors to date.

There are a few methods to separate the enantiomers. The first way is by using crystallisation; it is possible to crystallise only one isomer using a suitable solvent. If this does not work, chiral resolution is a technique that can be tried. This is a known process in stereochemistry to separate enantiomers of racemic mixtures.

In chiral resolution, a reaction of the racemic compound with a chiral enantiomerically pure derivatising reagent is carried out to make diastereomers. Diastereomers are known to be separable by conventional crystallisation or HPLC. This technique is also applied in a modern-day method in the synthesis of Duloxetine [29]. A potential way to separate the enantiomers is by using Mosher's acid, a derivatising agent. This can be reacted with **3G** to form an amide, allowing the enantiomers to be separated and then hydrolysed under strongly alkaline conditions to yield pure **R-3G** and **S-3G** [30].

The synthesised derivatives and the two fragments of **10115** have not been tested yet. Therefore, it remains unknown what the exact  $\text{IC}_{50}$  values of the derivatives will be. Once the compounds have been tested using the fluorescence assay, the data will be used in a docking study. In this way, we combine the earlier described DEL and hit optimisation techniques to find novel OGT inhibitor scaffolds with high target affinities. Short term docking studies will focus on finding different substituents in the  $\text{R}_1$ , 2 and 3 positions to improve target affinity or physiochemical properties.

## 6. Conclusion

In this research, we successfully synthesised five derivatives of **Vs-51**, with compound **6A<sub>1</sub>** having an  $\text{IC}_{50}$  of  $27 \pm 13 \mu\text{M}$  being the most potent. Even though two of the five compounds have not been tested with the fluorescence activity assay yet, we have already improved our insight into improving **Vs-51** as an OGT inhibitor. It has been found that extending the inhibitor with an extra ring in the  $\text{R}_2$  position leads to complete loss of inhibitory activity;

however, adding a furan in R<sub>1</sub> lead to an increase in inhibitory activity. Installing chlorine in R<sub>3</sub> to mimic the cation-dipole interaction of OSMI-4 didn't result in improved activity and even led to solubility issues. These results will be used in further hit optimisation studies to improve the **Vs-51** scaffold.

The second part of this research successfully designed a synthesis route to make **10115**. The designed synthetic route allows the synthesis of numerous more derivatives of **10115**; in this research, already four are synthesised and form a small library. This library can then be used in a hit optimisation study to improve the inhibitory effect of the **10115** scaffolds. At last, a promising method for separating the enantiomers, chiral resolution, can improve target affinity by getting the enantioselective compounds. Thereby potentially getting **10115** up with the most potent OGT inhibitors up to date.

### Supporting Information

In the Supplementary data, all the obtained <sup>1</sup>H-NMR and <sup>13</sup>C-NMR spectra from this study are presented. [Supplementary data](#)

### Experimental section

All reagents and solvents were commercially available and used without further purification. Water used for isolations was purified. Column chromatography was carried out on silica gel 60 Merck 0.040–0.063 mm. <sup>1</sup>H NMR and <sup>13</sup>C NMR spectra were recorded using an Agilent 400-MR spectrometer operating at 400 MHz for <sup>1</sup>H and 101 MHz for <sup>13</sup>C. Alternatively, they were recorded using a Bruker 600 UltraShield spectrometer operating at 600 MHz for <sup>1</sup>H and 151 MHz for <sup>13</sup>C. The chemical shifts ( $\delta$  values) and coupling constants ( $J$  values) are given in ppm and hertz (Hz), respectively. HPLC analysis was performed on a Thermo Scientific Dionex UltiMate 3000 system (Thermo Fisher Scientific Inc., Waltham, MA, USA), using an Accucore C<sub>18</sub> column (2.6  $\mu$ m, 100  $\times$  4.6 mm), at a flow rate of 0.8 mL/min, temperature 45°C and injection volume of 5  $\mu$ L. Method: The eluent was a mixture of 0.1% TFA in 95% water/acetonitrile (A) and 0.1% TFA 95% acetonitrile/water (B). The gradient was 0% B for 2 min, then to 100% B in 50 min, and then 100% B for 2 min. The purity of all the tested compounds was established to be  $\geq$ 95%, except for **6A<sub>1</sub>** (92%) and **6A<sub>2</sub>** (75%).

### Fluorescence activity assay

The fluorescence activity assay was performed as published before [31]. OGT reactions were carried out in a final volume of 25  $\mu$ L, containing 2.8  $\mu$ M glycosyl donor; BFL-UDP-GlcNAc, 50–200 nM of purified full-length OGT, 9.2  $\mu$ M glycosyl acceptor HCF-1 serine in OGT reaction buffer which is 1x PBS pH:7.4, 1 mM DTT, 12.5 mM MgCl<sub>2</sub>. These reactions were incubated at RT for 1 hour in the presence of different concentrations of inhibitors, which were first incubated with OGT for 5 minutes. Then the reactions were stopped by a mix of UDP (final concentration 2mM) and a solution of Nanolink® magnetic streptavidin beads (Vector Laboratories, Burlingame, CA, USA). This was incubated at RT for 30 minutes, and next, the beads were immobilised on a magnetic surface and

washed with PBS-tween 0,01%. At last, the beads were resuspended in PBS-tween 0,01% and transferred into a microplate. A POLARstarR® Omega microplate reader (BMG LABTECH, Ortenberg, Germany) or a Synergie H4 Hybrid Reader (BioTek, Winooski, VT, USA) were used for reading the fluorescence at Ex/Em= 485/530. This data was then normalised and plotted with GraphPad Prism 8.2.1 software. The IC<sub>50</sub> was calculated using a nonlinear regression-based fitting of the inhibition curves using the (inhibitor) against response-variable slope (four parameters).

### Synthesis of Vs-51 derivatives

#### 2-acetyl-N-(p-tolyl) hydrazine-1-carbothioamide (4A)

4-tosyl thiocyanate (291 mg, 1,95 mmol) and acetyl hydrazide (154 mg, 2,07 mmol) were dissolved in 4 mL ethanol and refluxed for 3 h. TLC was used to monitor the reaction (100% EtOAc). The mixture was allowed to crystallise overnight at 4–7 °C. The formed crystals were filtered off and dried. This resulted in white crystals (yield: 87%).

<sup>1</sup>H NMR (400 MHz, DMSO)  $\delta$  9.83 (s, 1H), 9.52 (s, 1H), 9.43 (s, 1H), 7.28 (d,  $J$  = 8.0 Hz, 2H), 7.13 (d,  $J$  = 8.1 Hz, 2H), 2.28 (s, 3H), 1.88 (s, 3H).

#### 5-methyl-4-(p-tolyl)-2,4-dihydro-3H-1,2,4-triazole-3-thione (5A)

**4A** (379 mg, 1,7 mmol) was dissolved in 5 mL 2N NaOH solution (H<sub>2</sub>O: EtOH) and refluxed for 3 h. TLC was used to monitor the reaction (100% EtOAc). When the reaction was completed, the mixture was acetylated to pH=4 by a 37% HCl solution; a white precipitate was formed. The precipitate was filtered off and dried. This resulted in a white solid (yield: 84%).

<sup>1</sup>H NMR (400 MHz, DMSO)  $\delta$  7.36 (d,  $J$  = 8.1 Hz, 2H), 7.32 – 7.26 (m, 2H), 2.39 (s, 3H), 2.08 (s, 3H).

#### 5-(2-((5-methyl-4-(p-tolyl)-4H-1,2,4-triazol-3-yl)thio)acetyl)indolin-2-one (6A1)

**5A** (95,4 mg, 0,465 mmol), 5-(chloroacetyl) oxindole (127 mg, 0,606 mmol) and sodium bicarbonate (41,2 mg; 0,49 mmol) were dissolved in 10 mL absolute ethanol and refluxed at 40 °C until TLC showed full conversion was achieved (1:15 MeOH: DCM). Then the mixture was concentrated, and ice was added to the mixture and stirred until it was completely molten. The formed precipitate was filtered off and dried. The precipitate was purified using column chromatography (1:30 MeOH: DCM). The product was concentrated and dried. This resulted in a pale pink solid (yield: 79%). NMR spectra showed solvent traces.

<sup>1</sup>H NMR (400 MHz, DMSO)  $\delta$  10.81 (s, 1H), 7.89 (dd,  $J$  = 8.2, 1.9 Hz, 1H), 7.85 – 7.80 (m, 1H), 7.44 – 7.36 (m, 2H), 7.36 – 7.28 (m, 2H), 6.92 (dd,  $J$  = 8.2, 3.5 Hz, 1H), 4.76 (s, 2H), 3.57 (s, 2H), 2.40 (s, 3H), 2.18 (s, 3H).

<sup>13</sup>C NMR (151 MHz, DMSO)  $\delta$  191.67, 176.74, 152.38, 149.21, 148.90, 139.64, 130.57, 130.37, 129.69, 128.76, 126.80, 126.23, 124.59, 108.83, 40.01, 35.48, 20.74, 10.83.



**6-chloro-5-(2-((5-methyl-4-(p-tolyl)-4H-1,2,4-triazol-3-yl) thio) acetyl) indolin-2-one (6A2)**

The same method as for **6A<sub>1</sub>** was used, but 1,2 eq. (138 mg, 0,57 mmol) of 6-chloro-5-(2-chloroacetyl) indolin-2-one was added to **5A** (0,0961g; 0,4681 mmol). This resulted in a pink solid (yield: 63%). NMR spectra showed solvent traces.

<sup>1</sup>H NMR (600 MHz, DMSO) δ 10.83 (s, 1H), 7.72 (s, 1H), 7.40 (d, J = 8.0 Hz, 2H), 7.31 (d, J = 7.9 Hz, 2H), 6.90 (s, 1H), 4.70 (s, 2H), 3.56 (s, 2H), 2.40 (d, J = 5.5 Hz, 3H), 2.18 (s, 3H).

<sup>13</sup>C NMR (151 MHz, DMSO) δ 193.26, 176.53, 152.41, 149.07, 148.07, 139.68, 131.16, 131.10, 130.48, 130.39, 128.38, 127.38, 126.74, 126.67, 126.54, 126.14, 125.06, 110.84, 40.06, 20.74, 10.81.

**4-(nitrophenyl) morpholine (1B)**

1-fluoro-4-nitrobenzene (1,01 g, 7,19 mmol), morpholine (1 mL, 11,59 mmol) and triethylamine (3 mL, 21,52 mmol) were dissolved in 7,5 mL acetonitrile and refluxed at 80 °C for 3 h. TLC was used to monitor the reaction (EtOAc: PE 1:5). The reaction was slowly cooled and poured into 30 mL of water and extracted twice with 30 mL EtOAc. The organic layers were combined and washed with a brine solution, dried over sodium sulfate, and concentrated. This resulted in a yellow solid (yield: 86%).

<sup>1</sup>H NMR (400 MHz, CDCl<sub>3</sub>) δ 8.19 – 8.10 (m, 2H), 6.88 – 6.79 (m, 2H), 3.90 – 3.83 (m, 4H), 3.41 – 3.34 (m, 4H).

**4-merpholinoaniline (2B)**

**1B** (1,28 g, 6,15 mmol) was dissolved in 20 mL technical ethanol and flushed with argon for 10 minutes. Then 10 m/m% Pd/C complex was added to the mixture and was stirred overnight under hydrogen. TLC was used to monitor the reaction (EtOAc: PE 1:1). Once the reaction was complete, the Pd/C complex was filtered off, and the filtrate was concentrated to yield a purple solid (yield: 87%). NMR spectra showed solvent traces.

<sup>1</sup>H NMR (400 MHz, DMSO) δ 6.70 – 6.64 (m, 2H), 6.52 – 6.45 (m, 2H), 4.56 (s, 2H), 3.70 – 3.65 (m, 4H), 2.89 – 2.82 (m, 4H).

**4-(4-isothiocyanatophenyl) Morpholine (3B)**

**2B** (489 mg, 2,74 mmol) and triethylamine (1 mL, 7,17 mmol) were dissolved in 5 mL THF. Argon was flushed through the solution for 10 minutes. Then, carbon disulphide (0,4 mL, 6,62 mmol) was slowly added to the solution while cooled with an ice bath. The reaction was stirred overnight and monitored by TLC (EtOAc: PE 1:1). When **2B** was converted into the dithiocarbamate salt, tosyl chloride (695 mg, 3,64 mmol) was added to the mixture and stirred for 1 hour. When the dithiocarbamate salt was converted into the corresponding isothiocyanate, the mixture was poured into a 1M HCl solution (10 mL) and extracted three times with 10 mL MTBE. The organic layers were combined, dried, and concentrated. Then tosyl chloride was removed from the mixture by column chromatography; first, 100% PE was used to elute tosyl chloride, and then 5:1 PE: EtOAc was used to elute **3B**. The product was concentrated and dried to yield a pale-yellow solid (70%).

<sup>1</sup>H NMR (400 MHz, DMSO) δ 7.31 – 7.22 (m, 2H), 6.97 – 6.88 (m, 2H), 3.72 – 3.65 (m, 4H), 3.15 – 3.08 (m, 4H).

**2-(furan-2-carbonyl)-N-(4-morpholinophenyl) hydrazine-1-carbothioamide (4B)**

**3B** (418 mg, 1,9 mmol) and 2-furoic hydrazide (248 mg, 1,97 mmol) were dissolved in 10 mL ethanol and refluxed for 3 h. TLC was used to monitor the reaction (5:1 PE: EtOAc). The mixture was allowed to crystallise overnight at 4–7 °C. The formed crystals were filtered off and dried. This resulted in off-white crystals (yield: 75%). NMR spectra showed solvent traces.

<sup>1</sup>H NMR (400 MHz, DMSO) δ 10.36 (s, 1H), 9.64 (s, 1H), 9.51 (s, 1H), 7.90 (dd, J = 1.8, 0.8 Hz, 1H), 7.25 (s, 2H), 7.22 (s, 1H), 6.89 (d, J = 9.0 Hz, 2H), 6.66 (dd, J = 3.5, 1.7 Hz, 1H), 3.73 (dd, J = 6.0, 3.6 Hz, 4H), 3.11 – 3.01 (m, 4H).

**2-(furan-2-yl)-4-(4-morpholinophenyl)-2,4-dihydro-3H-pyrazole-3-thione (5B)**

**4B** (444 mg, 1,28 mmol) was dissolved in 5 mL 2N NaOH solution (H<sub>2</sub>O: EtOH) and refluxed for 3 h. TLC was used to monitor the reaction (100% EtOAc). When the reaction was completed, the mixture was acetified to pH=4 by a 37% HCl solution; a white precipitate was formed. The precipitate was filtered off and dried. This resulted in a white solid (yield: 88%). NMR spectra showed solvent traces.

<sup>1</sup>H NMR (400 MHz, DMSO) δ 7.82 (d, J = 1.8 Hz, 1H), 7.22 (d, J = 8.9 Hz, 2H), 7.08 (d, J = 8.6 Hz, 2H), 6.51 (dd, J = 3.6, 1.8 Hz, 1H), 5.88 (d, J = 3.4 Hz, 1H), 3.76 (t, J = 4.8 Hz, 4H), 3.23 (t, J = 4.9 Hz, 4H).

**5-(2-((5-(furan-2-yl)-4-(4-morpholinophenyl)-4H-1,2,4-triazol-3-yl) thio) acetyl) indolin-2-one (6B<sub>1</sub>)**

**5B** (50,6 mg, 0,155 mmol), 5-(chloroacetyl) oxindole (40,3 mg, 0,192 mmol) and sodium bicarbonate (13,1 mg, 0,156 mmol) were dissolved in 10 mL absolute ethanol and refluxed at 40 °C until TLC showed full conversion was achieved (1:15 MeOH: DCM). Then the mixture was concentrated, and ice was added to the mixture and stirred until it was completely molten. The formed precipitate was filtered off and dried. The precipitate was purified using column chromatography (1:30 MeOH: DCM). The product was concentrated and dried. This resulted in a pale pink solid (yield: 35%). NMR spectra showed solvent traces.

<sup>1</sup>H NMR (600 MHz, DMSO) δ 10.83 (s, 1H), 7.92 (ddd, J = 8.3, 1.8, 0.9 Hz, 1H), 7.85 (t, J = 1.3 Hz, 1H), 7.78 (dd, J = 1.8, 0.8 Hz, 1H), 7.32 – 7.26 (m, 2H), 7.12 – 7.07 (m, 2H), 6.93 (d, J = 8.2 Hz, 1H), 6.52 (dd, J = 3.5, 1.8 Hz, 1H), 6.09 (dd, J = 3.5, 0.8 Hz, 1H), 4.85 (s, 2H), 3.78 – 3.74 (m, 4H), 3.58 (s, 2H), 3.26 – 3.22 (m, 4H).

<sup>13</sup>C NMR (151 MHz, DMSO) δ 192.13, 177.23, 152.35, 152.25, 148.07, 145.16, 141.58, 130.22, 129.21, 128.63, 126.74, 125.10, 123.83, 115.42, 112.07, 111.43, 109.34, 66.44, 47.84, 35.97, 29.46 (d, J = 6.4 Hz).

**4-(nitrophenyl) piperazine (1D)**

1-fluoro-4-nitrobenzene (880,1 mg, 6,24 mmol), piperazine (1,725 g, 20,03 mmol) and triethylamine (2,25 mL, 16,14 mmol) were dissolved in 7,5 mL acetonitrile and refluxed at 80 °C for 3 h. TLC was used to monitor the reaction (EtOAc: PE 1:1). The reaction was slowly cooled, poured into 30 mL of water, and extracted four times with 30 mL EtOAc. The organic layers were combined and washed with a brine solution, dried over sodium sulphate, and concentrated. The product was purified using column chromatography; first, 1:1 PE: EtOAc was used to elute the side product, and then 10% MeOH in DCM was used to elute **1D**. Then the product was concentrated and dried, resulting in a yellow solid (yield: 96%).

$^1\text{H NMR}$  (400 MHz, DMSO)  $\delta$  8.08 – 7.99 (m, 2H), 7.04 – 6.95 (m, 2H), 3.36 (dd,  $J = 4.3, 2.6$  Hz, 4H), 2.83 – 2.76 (m, 4H).

**1-Boc-4-(4-Nitrophenyl) piperazine (2D)**

**1D** (1,233 g, 5,95 mmol) and di-*tert*-butyl-dicarbonate (1,46 g, 6,71 mmol) were dissolved in 10 mL demineralized water and stirred for 1 hour. After TLC showed that **2D** was formed, ammonia (0,25 mL, 6,28 mmol) was added to the solution and stirred for 1 hour. Then **2D** was filtered off, washed with water, and dried under a high vacuum; this resulted in a yellow solid (yield: 96%).

$^1\text{H NMR}$  (400 MHz, DMSO)  $\delta$  8.12 – 8.03 (m, 2H), 7.06 – 6.97 (m, 2H), 3.48 (s, 8H), 1.43 (s, 9H).

**4-(4-Boc-piperazin-1-yl) aniline (3D)**

**2D** (1,1 g, 3,58 mmol) was dissolved in 20 mL technical ethanol and flushed with argon for 10 minutes. Then 10 m/m% Pd/C complex was added to the mixture and was stirred overnight under hydrogen. TLC was used to monitor the reaction (EtOAc: PE 1:1). Once the reaction was complete, the Pd/C complex was filtered off, and the filtrate was concentrated to yield a purple solid (yield: 96,6%).

$^1\text{H NMR}$  (400 MHz, DMSO)  $\delta$  6.72 – 6.67 (m, 2H), 6.52 – 6.46 (m, 2H), 4.60 (s, 2H), 3.41 (t,  $J = 5.1$  Hz, 4H), 2.86 – 2.79 (m, 4H), 1.41 (s, 9H).

**1-Boc- 4-(4-isothiocyanatophenyl) piperazine (4D)**

**3D** (488,6 mg, 2,74 mmol) and triethylamine (1 mL, 7,17 mmol) were dissolved in 5 mL THF. Argon was flushed through the solution for 10 minutes. Then, carbon disulphide (0,4 mL, 6,62 mmol) was slowly added to the solution while cooled with an ice bath. The reaction was stirred overnight and monitored by TLC (EtOAc: PE 1:1). When **2B** was converted into the dithiocarbamate salt, tosyl chloride (695 mg, 3,64 mmol) was added to the mixture and stirred for 1 hour. When the dithiocarbamate salt was converted into the corresponding isothiocyanate, the mixture was poured into a 1M HCl solution (10 mL) and extracted three times with 10 mL MTBE. The organic layers were combined, dried, and concentrated. Then tosyl chloride was removed from the mixture by column chromatography; first, 100% PE was used to elute tosyl chloride, and then 5:1 PE: EtOAc was used to elute **4D**. The product was concentrated and dried to yield a pale-yellow solid (70%). NMR spectra showed solvent traces.

$^1\text{H NMR}$  (400 MHz, DMSO)  $\delta$  7.34 – 7.25 (m, 2H), 7.00 – 6.92 (m, 2H), 3.43 (dd,  $J = 6.4, 3.9$  Hz, 5H), 3.17 (dd,  $J = 6.4, 4.0$  Hz, 4H), 1.41 (s, 9H).

**2-acetyl-N-(4-morpholinophenyl) hydrazine-1-carbothioamide (5D)**

**4D** (1,02 g, 3,19 mmol) and furoic hydrazide (422 mg, 3,3 mmol) were dissolved in 10 mL ethanol and refluxed for 3 h. Then the mixture was slowly cooled to room temperature and left in the fridge the crystallise overnight. A pale-yellow solid was filtered off and dried (yield: 61%). NMR spectra showed solvent traces.

$^1\text{H NMR}$  (400 MHz, DMSO)  $\delta$  10.34 (s, 0H), 9.60 (s, 1H), 9.49 (s, 0H), 7.88 – 7.83 (m, 1H), 7.19 (t,  $J = 7.5$  Hz, 3H), 6.86 (d,  $J = 8.9$  Hz, 2H), 6.63 (dd,  $J = 3.5, 1.7$  Hz, 1H), 3.43 – 3.40 (m, 4H), 3.03 (t,  $J = 5.2$  Hz, 4H), 1.38 (s, 9H).

**5-(furan-2-yl)-4-(4-(piperazin-1-yl) phenyl)-2,4-dihydro-3H-1,2,4-triazole-3-thione (6D)**

**5D** (700 mg, 1,57 mmol) was dissolved in 2N NaOH solution (H<sub>2</sub>O: EtOH) and refluxed for 3 h. TLC was used to monitor the reaction (1:1 EtOAc: PE). When the reaction was complete, the mixture was acetylated to pH=4 by a 37% HCl solution and a white precipitate was formed. The suspension was filtered, and the filtrate was stirred in 1 M HCl solution for 1 hour to deprotect the compound (TLC was used to monitor the deprotection). Then, the white solid was filtered off, washed with water, and dried to yield the desired compound (yield: 66%). NMR spectra showed solvent traces.

$^1\text{H NMR}$  (400 MHz, DMSO)  $\delta$  7.83 (dd,  $J = 1.8, 0.7$  Hz, 1H), 7.28 (d,  $J = 9.0$  Hz, 2H), 7.14 (d,  $J = 9.0$  Hz, 2H), 6.52 (dd,  $J = 3.5, 1.8$  Hz, 1H), 5.89 (dd,  $J = 3.5, 0.8$  Hz, 1H), 3.47 (t,  $J = 5.2$  Hz, 4H), 3.27 (d,  $J = 5.4$  Hz, 4H).

**5-(2-((5-(furan-2-yl)-4-(4-(piperazin-1-yl) phenyl)-4H-1,2,4-triazol-3-yl) thio) acetyl) indolin-2-one (7D<sub>1</sub>)**

**6D** (50,7 mg, 0,15 mmol), 5-(chloroacetyl) oxindole (34,7 mg, 0,16 mmol) and potassium carbonate (22 mg, 0,16 mmol) were dissolved in 3 mL absolute ethanol under argon. The mixture was stirred at RT for 72 h and turned from a white to a light pink suspension. TLC was used to monitor the reaction (1:15 MeOH: DCM + Et<sub>3</sub>N). Then the mixture was concentrated, and the residue was stirred in ice. When a suspension in water was formed, the solid was filtered off and washed with cold water. Then the product was dissolved in a 1:30 MeOH: DCM mixture and ran on a silica column with the respective eluent. When the indole was eluted, Et<sub>3</sub>N was added to the eluent to elute compound **7D<sub>1</sub>**, which after concentrating the fractions, yielded a light pink solid (yield: 93%).

$^1\text{H NMR}$  (600 MHz, DMSO)  $\delta$  10.83 (s, 1H), 7.92 (dd,  $J = 8.1, 1.8$  Hz, 1H), 7.85 (s, 1H), 7.78 (d,  $J = 1.6$  Hz, 1H), 7.30 – 7.19 (m, 2H), 7.12 – 7.05 (m, 2H), 6.94 (d,  $J = 8.2$  Hz, 1H), 6.54 – 6.50 (m, 1H), 6.08 (d,  $J = 3.6$  Hz, 1H), 4.85 (s, 2H), 3.58 (s, 2H), 3.20 (t,  $J = 5.1$  Hz, 4H), 2.88 (t,  $J = 5.1$  Hz, 4H).

$^{13}\text{C NMR}$  (101 MHz, DMSO)  $\delta$  191.66, 176.77, 152.21, 151.83, 148.96, 147.63, 144.67, 141.12, 129.75, 128.75,

128.10, 126.27, 124.63, 122.88, 115.06, 111.59, 110.95, 108.88, 47.92, 45.21, 35.50.

**6-chloro-5-(2-((5-(furan-2-yl)-4-(4-(piperazin-1-yl)phenyl)-4H-1,2,4-triazol-3-yl) thio) acetyl) indolin-2-one (7D<sub>2</sub>)**

The same method as for **7D<sub>1</sub>** was used, but now 6-chloro-5-(2-chloroacetyl) indolin-2-one (21,2 mg, 0,087 mmol) was added to **6D** (27 mg; 0,083 mmol). This resulted in a pink solid (yield: 98%).

<sup>1</sup>H NMR (600 MHz, DMSO) δ 10.81 (s, 1H), 7.78 (d, J = 1.8 Hz, 1H), 7.76 (s, 1H), 7.27 – 7.22 (m, 2H), 7.10 – 7.07 (m, 2H), 6.92 (s, 1H), 6.52 (dd, J = 3.5, 1.8 Hz, 1H), 6.09 (d, J = 3.5 Hz, 1H), 4.78 (s, 2H), 3.57 (s, 2H), 3.25 (t, J = 5.2 Hz, 4H), 2.94 (t, J = 5.2 Hz, 4H).

**Synthesis of 10115 derivatives**

**N-methoxy-N-methyl-[1,1'-biphenyl]-4-carboxamide (1G)**

4-biphenylcarbonyl chloride (9,98 g 46,19 mmol) and N,O-dimethylhydroxylamine (4,67 g, 47,91 mmol) were dissolved in DCM and put in an ice bath. Then triethylamine (13 mL, 93,27 mmol) was added slowly, and the suspension was stirred overnight. Once TLC showed complete conversion, the reaction was quenched with 20 mL of saturated ammonium chloride solution and stirred for 30 minutes. Then, the aqueous phase was extracted with DCM and then extracted with brine. Subsequently, the organic phase was dried using magnesium sulphate and then concentrated and dried. The product was purified using column chromatography with 30% EtOAc in PE (yield: 82%). NMR spectra showed solvent traces.

<sup>1</sup>H NMR (400 MHz, CDCl<sub>3</sub>) δ 7.82 – 7.74 (m, 2H), 7.67 – 7.58 (m, 4H), 7.51 – 7.42 (m, 2H), 7.42 – 7.34 (m, 1H), 3.60 (s, 3H), 3.39 (s, 3H).

**[1,1'-biphenyl]-4-carbaldehyde (2G)**

**1G** (9,1 g, 37,74 mmol) was dissolved in THF and cooled down to -78 °C using dry ice. Then, 1M LiAlH<sub>4</sub> in THF (44 mL, 44 mmol) was added in small portions over 1 hour. After 1 hour of stirring, the reaction was allowed to warm to 4 °C slowly and stirred overnight. The reaction was monitored using TLC (which required small work up) using 50% EtOAc in PE as an eluent. Once the reaction did not proceed, it was quenched with a 10% potassium bisulphate solution at 4 °C and allowed to RT. Then the product was concentrated, and water was added to the mixture. Then it was extracted using ethyl acetate three times, and then the organic phase was extracted using brine once. Subsequently, the organic layer was dried using magnesium sulphate and concentrated and dried to yield **2G** (yield: 93%). NMR spectra showed solvent traces.

<sup>1</sup>H NMR (400 MHz, CDCl<sub>3</sub>) δ 10.06 (s, 1H), 8.00 – 7.92 (m, 2H), 7.80 – 7.72 (m, 2H), 7.68 – 7.62 (m, 2H), 7.53 – 7.45 (m, 2H), 7.45 – 7.40 (m, 1H).

**3-([1,1'-biphenyl]-4-yl)-3-aminopropanoic acid (3G)**

**2G** (6,4 g, 35,15 mmol), malonic acid (4,22 g, 40,56 mmol) and ammonium acetate (6,67 g, 86,55 mmol) were dissolved in ethanol. This was then refluxed overnight, after which a

white precipitate was formed. The reaction was allowed to cool down to RT, and the precipitate was collected by vacuum filtration and washed with ethanol. Then the precipitated was dried and analysed (yield: 35%). NMR spectra showed solvent traces. <sup>1</sup>H NMR (400 MHz, D<sub>2</sub>O + K<sub>2</sub>CO<sub>3</sub>) δ 7.73 (t, J = 8.0 Hz, 4H), 7.53 (t, J = 8.3 Hz, 4H), 7.46 (d, J = 7.8 Hz, 1H), 4.34 (d, J = 7.7 Hz, 1H), 2.63 (d, J = 7.5 Hz, 2H).

**Ethyl 3-([1,1'-biphenyl]-4-yl)-3-aminopropanoate (4G)**

**3G** (225 mg, 1,06 mmol) was suspended in ethanol and cooled using an ice bath. Then thionyl chloride (0,09 mL, 3,22 mmol) was slowly added to the reaction, upon which a clear solution formed. This was refluxed for 3 h until TLC showed the reaction was over. The reaction was cooled down to RT and concentrated and purified using column chromatography using 70% EtOAc/PE as an eluent (92%). NMR spectra showed solvent traces.

<sup>1</sup>H NMR (400 MHz, CDCl<sub>3</sub>) δ 8.91 (s, 2H), 7.68 – 7.53 (m, 4H), 7.50 (d, J = 7.4 Hz, 2H), 7.36 (dt, J = 13.4, 7.0 Hz, 3H), 4.80 (s, 1H), 4.12 – 3.93 (m, 2H), 3.30 (s, 1H), 3.09 (s, 1H), 1.10 (s, 3H).

**Tert-butyl 5-(4-bromophenyl) nicotinate (1H)**

5-(4-bromophenyl) nicotinic acid (250 mg, 0,903 mmol) and DMAP (224 mg, 0,183 mmol) were dissolved in THF and put under reflux. Then, di-*tert*-butyl decarbonate (494,5 mg, 2,267 mmol) was dissolved in THF and dropwise added to the reaction. This mixture was refluxed for 4 h and monitored using TLC. Once the reaction was completed, the reaction was allowed to cool down to RT and concentrated. Then the residue was dissolved in MTBE and extracted with; demi-water, 1 M phosphoric acid, demi-water, 10% sodium carbonate solution and brine. Then the organic layer was dried using magnesium sulphate and concentrated to yield **1H** (yield: 55%).

<sup>1</sup>H NMR (400 MHz, CDCl<sub>3</sub>) δ 9.15 (d, J = 2.0 Hz, 1H), 8.93 (d, J = 2.3 Hz, 1H), 8.39 (t, J = 2.2 Hz, 1H), 7.68 – 7.60 (m, 2H), 7.53 – 7.45 (m, 2H), 1.63 (s, 9H).

**Tert-butyl 5-(4-(furan-2-yl)phenyl)nicotinate (2H)**

**1H** (165 mg, 0,495 mmol) and Pd(dppf)Cl<sub>2</sub> (16,5 mg, 0,028 mmol) and sodium *tert*-butoxide (53,2 mg, 0,55 mmol) were dissolved in 90% THF in water. Next, a vacuum was pulled inside the setup, which was then flushed with argon, this was repeated three times, and then the reaction was put under reflux. After this, a droplet funnel was used to add furan-2-boronic acid (62,2 mg, 0,56 mmol) over 1 hour and allowed to reflux overnight. Once TLC showed the reaction was not proceeding anymore, the reaction was cooled to RT and concentrated. Then water was added and extracted using DCM, after which the organic layer was washed using brine, dried over magnesium sulphate, concentrated, and dried. Column chromatography was used to purify **2H** using 30% EtOAc/PE as eluent (yield: 59%)

<sup>1</sup>H NMR (400 MHz, CDCl<sub>3</sub>) δ 9.13 (d, J = 2.0 Hz, 1H), 9.00 (d, J = 2.3 Hz, 1H), 8.45 (t, J = 2.2 Hz, 1H), 7.84 – 7.77 (m, 2H), 7.69 – 7.61 (m, 2H), 7.54 – 7.49 (m, 1H),

6.74 (dd,  $J = 3.4, 0.8$  Hz, 1H), 6.52 (dd,  $J = 3.4, 1.8$  Hz, 1H), 1.64 (s, 9H).

### 5-(4-(furan-2-yl)phenyl)nicotinic acid (3H)

**2H** (85,8 mg, 0,037 mmol) was dissolved in 10 mL DCM and cooled using an ice bath, then 1 mL of TFA was added, and the mixture was allowed to stir overnight at RT. Once TLC showed full deprotection of **2H**, the mixture was concentrated, and column chromatography was used to purify **3H** using 10% MeOH/DCM and triethylamine (yield: 92%).

$^1\text{H NMR}$  (400 MHz, DMSO)  $\delta$  9.05 (s, 2H), 8.48 (s, 1H), 7.85 (s, 4H), 7.80 (d,  $J = 1.8$  Hz, 1H), 7.07 (d,  $J = 3.2$  Hz, 1H), 6.64 (dd,  $J = 3.4, 1.8$  Hz, 1H).

### Ethyl 3-([1,1'-biphenyl]-4-yl)-3-(5-(4-bromophenyl)nicotinamido)propanoate (5G)

5-(4-bromophenyl) nicotinic acid (11 mg, 0,04 mmol), HATU (18,3 mg, 0,048 mmol) and DIPEA (0,011 mL, 0,115 mmol) were dissolved in 2 mL DMF and stirred for 30 mins at RT. Then, **4G** (12 mg, 0,045 mmol) was dissolved in 1 mL DMF and slowly added to the mixture. The reaction was stirred for 48 h, concentrated under vacuo and dried. Purification was done using column chromatography with 30% EtOAc/PE as eluent (yield: 53%). NMR spectra showed solvent traces.

$^1\text{H NMR}$  (600 MHz,  $\text{CDCl}_3$ )  $\delta$  9.11 (s, 1H), 8.99 (s, 1H), 8.58 (s, 1H), 8.07 (d,  $J = 8.1$  Hz, 1H), 7.69 – 7.64 (m, 2H), 7.60 – 7.53 (m, 4H), 7.53 – 7.48 (m, 2H), 7.47 – 7.40 (m, 4H), 7.39 – 7.32 (m, 1H), 5.69 (dt,  $J = 8.0, 5.7$  Hz, 1H), 4.15 (q,  $J = 7.1$  Hz, 2H), 3.08 (dd,  $J = 15.9, 5.9$  Hz, 1H), 3.01 (dd,  $J = 15.9, 5.6$  Hz, 1H), 1.21 (t,  $J = 7.1$  Hz, 3H).

$^{13}\text{C NMR}$  (151 MHz,  $\text{CDCl}_3$ )  $\delta$  171.70, 163.19, 140.94, 140.44, 138.94, 134.21, 132.76, 128.83, 128.75, 127.61, 127.50, 127.06, 126.75, 124.14, 61.27, 50.26, 39.53, 14.10 (d,  $J = 7.6$  Hz).

### Ethyl 3-([1,1'-biphenyl]-4-yl)-3-(5-(4-(furan-2-yl)phenyl)nicotinamido)propanoate (6G)

Compound **6G** was synthesised using the same method described for **5G** but it was done using compound **3H** (21 mg, 0,076 mmol) and **4G** (24,4 mg, 0,091 mmol). This resulted in a pale-yellow solid (yield: 54%). NMR spectra showed solvent traces.

$^1\text{H NMR}$  (400 MHz,  $\text{CDCl}_3$ )  $\delta$  9.01 (dd,  $J = 5.6, 2.2$  Hz, 2H), 8.38 (t,  $J = 2.2$  Hz, 1H), 7.80 (d,  $J = 8.4$  Hz, 2H), 7.76 (d,  $J = 8.4$  Hz, 1H), 7.66 (d,  $J = 8.4$  Hz, 2H), 7.58 (t,  $J = 8.2$  Hz, 4H), 7.54 – 7.49 (m, 1H), 7.49 – 7.40 (m, 4H), 7.35 (t,  $J = 7.4$  Hz, 1H), 6.77 – 6.71 (m, 1H), 6.51 (dd,  $J = 3.4, 1.8$  Hz, 1H), 5.75 – 5.68 (m, 1H), 4.15 (q,  $J = 7.1$  Hz, 2H), 3.14 – 2.97 (m, 2H), 1.21 (t,  $J = 7.1$  Hz, 3H).

### Ethyl 3-(4-bromophenyl)-3-(5-(4-(furan-2-yl)phenyl)nicotinamido)propanoate (5H)

Compound **5H** was synthesized using the same method described for **5G** but it was done using compound **3H** (18,5 mg, 0,07 mmol) and ethyl-3-amino-3-(4-bromophenyl)propanoate (24 mg, 0,089 mmol). This resulted in a pale-

yellow solid (yield: 23%). NMR spectra showed solvent traces.

$^1\text{H NMR}$  (600 MHz,  $\text{CDCl}_3$ )  $\delta$  9.16 – 8.99 (m, 2H), 8.60 (s, 1H), 8.08 – 8.01 (m, 1H), 7.82 (d,  $J = 8.3$  Hz, 1H), 7.66 (d,  $J = 8.3$  Hz, 2H), 7.52 (dd,  $J = 1.8, 0.7$  Hz, 1H), 7.51 – 7.46 (m, 2H), 7.46 – 7.40 (m, 1H), 7.28 (d,  $J = 8.5$  Hz, 2H), 7.16 (d,  $J = 8.3$  Hz, 1H), 6.77 (dd,  $J = 3.4, 0.8$  Hz, 1H), 6.52 (dd,  $J = 3.4, 1.8$  Hz, 1H), 5.59 (q,  $J = 6.2$  Hz, 1H), 4.13 (q,  $J = 7.2$  Hz, 2H), 1.21 (t,  $J = 7.1$  Hz, 3H).

### 3-([1,1'-biphenyl]-4-yl)-3-(5-(4-(furan-2-yl)phenyl)nicotinamido)propanoic acid (6G-A)

**6G** (10 mg, 0,019 mmol) was dissolved in 1 mL of ethanol, and 1 mL of 2M NaOH solution was added and refluxed for one hour. Once TLC showed the sodium salt was formed, the reaction was acidified (until pH=4) using a 6M HCl solution. Then the aqueous layer was extracted using ethyl acetate. Next, the organic layer is washed using brine, dried over magnesium sulphate and dried. This resulted in a yellow solid (yield: 99%). NMR spectra showed solvent traces.

### N-(1-([1,1'-biphenyl]-4-yl)-3-(methylamino)-3-oxopropyl)-5-(4-(furan-2-yl)phenyl)nicotinamide (10115)

**6G** (8,6 mg, 0,017 mmol) was dissolved in 1 mL methanol, to which 1 mL of 40% methylamine solution was added; this was stirred for 24h at RT. After TLC showed full conversion of **6G**, the reaction was concentrated and dried. This resulted in a beige solid (yield: 95%). NMR spectra showed solvent traces.

$^1\text{H NMR}$  (600 MHz, MeOD)  $\delta$  8.98 (s, 2H), 8.54 (s, 1H), 7.90 – 7.82 (m, 2H), 7.82 – 7.74 (m, 1H), 7.63 – 7.58 (m, 5H), 7.54 – 7.49 (m, 2H), 7.42 (t,  $J = 7.8$  Hz, 3H), 7.35 – 7.29 (m, 1H), 6.90 – 6.86 (m, 1H), 6.56 (dd,  $J = 3.4, 1.8$  Hz, 1H), 5.64 (t,  $J = 7.2$  Hz, 1H), 2.93 – 2.84 (m, 2H), 2.69 (d,  $J = 1.8$  Hz, 3H).

### Layman's summary

O-GlcNAcylation is a process inside cells that changes a protein's function, stability, and interactions. O-GlcNAc transferase (OGT) is an enzyme involved in this process. In some diseases, it is observed that O-GlcNAcylation is dysregulated, and therefore drugs are needed that decrease the activity of OGT. Inhibitors are small molecules that can occupy the functional space inside enzymes, reducing the activity. In the first part of this study, recently found inhibitors were improved to have higher activity, cell permeability or solubility. Improving these properties would make the compound more usable as a drug. This was done by changing side groups from the original structure. Unfortunately, this didn't lead to an improved compound, but still, a better insight was obtained on improving this compound in future studies. In the second part of this study, a synthetic route was designed to get a new inhibitor. This synthetic route allows the side groups to be changed in the final steps, which makes alterations of these groups easy. The compounds' tunability is significant because they can still be developed further to improve properties, like in the first part of this research.

## References

- Ju Kim, E. O -GlcNAc Transferase: Structural Characteristics, Catalytic Mechanism and Small-Molecule Inhibitors. *ChemBioChem* **2020**, *21*, 3026–3035, doi:10.1002/cbic.202000194.
- Yang, X.; Qian, K. Protein O-GlcNAcylation: Emerging Mechanisms and Functions. *Nat. Rev. Mol. Cell Biol.* **2017**, *18*, 452–465, doi:10.1038/nrm.2017.22.
- Levine, Z.G.; Walker, S. The Biochemistry of O-GlcNAc Transferase: Which Functions Make It Essential in Mammalian Cells? *Annu. Rev. Biochem.* **2016**, *85*, 631–657, doi:10.1146/annurev-biochem-060713-035344.
- Chang, Y.-H.; Weng, C.-L.; Lin, K.-I. O-GlcNAcylation and Its Role in the Immune System. *J. Biomed. Sci.* **2020**, *27*, 57, doi:10.1186/s12929-020-00648-9.
- Balsollier, C.; Pieters, R.J.; Anderluh, M. Overview of the Assays to Probe O-Linked  $\beta$ -n-Acetylglucosamine Transferase Binding and Activity. *Molecules* **2021**, *26*, doi:10.3390/molecules26041037.
- Bond, M.R.; Hanover, J.A. O- GlcNAc Cycling: A Link Between Metabolism and Chronic Disease. *Annu. Rev. Nutr.* **2013**, *33*, 205–229, doi:10.1146/annurev-nutr-071812-161240.
- Ma, Z.; Vosseller, K. O-GlcNAc in Cancer Biology. *Amino Acids* **2013**, *45*, 719–733, doi:10.1007/s00726-013-1543-8.
- Selnick, H.G.; Hess, J.F.; Tang, C.; Liu, K.; Schachter, J.B.; Ballard, J.E.; Marcus, J.; Klein, D.J.; Wang, X.; Pearson, M.; et al. Discovery of MK-8719, a Potent O-GlcNAcase Inhibitor as a Potential Treatment for Tauopathies. *J. Med. Chem.* **2019**, *62*, 10062–10097, doi:10.1021/acs.jmedchem.9b01090.
- Umaphathi, P.; Mesubi, O.O.; Banerjee, P.S.; Abrol, N.; Wang, Q.; Luczak, E.D.; Wu, Y.; Granger, J.M.; Wei, A.-C.; Reyes Gaido, O.E.; et al. Excessive O -GlcNAcylation Causes Heart Failure and Sudden Death. *Circulation* **2021**, *143*, 1687–1703, doi:10.1161/CIRCULATIONAHA.120.051911.
- Xu, W.; Zhang, X.; Wu, J.; Fu, L.; Liu, K.; Liu, D.; Chen, G.G.; Lai, P.B.; Wong, N.; Yu, J. O-GlcNAc Transferase Promotes Fatty Liver-Associated Liver Cancer through Inducing Palmitic Acid and Activating Endoplasmic Reticulum Stress. *J. Hepatol.* **2017**, *67*, 310–320, doi:10.1016/j.jhep.2017.03.017.
- Akella, N.M.; Minh, G. Le; Ciraku, L.; Mukherjee, A.; Bacigalupa, Z.A.; Mukhopadhyay, D.; Sodi, V.L.; Reginato, M.J. O-GlcNAc Transferase Regulates Cancer Stem like Potential of Breast Cancer Cells. *Mol. Cancer Res.* **2020**, *18*, 585–598, doi:10.1158/1541-7786.MCR-19-0732.
- Loi, E.M.; Tomašič, T.; Balsollier, C.; van Eekelen, K.; Weiss, M.; Gobec, M.; Alteen, M.G.; Vocadlo, D.J.; Pieters, R.J.; Anderluh, M. Discovery of a New Drug-Like Series of OGT Inhibitors by Virtual Screening. *Molecules* **2022**, *To be published*.
- Levine, Z.G.; Fan, C.; Melicher, M.S.; Orman, M.; Benjamin, T.; Walker, S. O -GlcNAc Transferase Recognizes Protein Substrates Using an Asparagine Ladder in the Tetratricopeptide Repeat (TPR) Superhelix. *J. Am. Chem. Soc.* **2018**, *140*, 3510–3513, doi:10.1021/jacs.7b13546.
- Jínek, M.; Rehwinkel, J.; Lazarus, B.D.; Izaurralde, E.; Hanover, J.A.; Conti, E. The Superhelical TPR-Repeat Domain of O-Linked GlcNAc Transferase Exhibits Structural Similarities to Importin  $\alpha$ . *Nat. Struct. Mol. Biol.* **2004**, *11*, 1001–1007, doi:10.1038/nsmb833.
- Lazarus, M.B.; Jiang, J.; Gloster, T.M.; Zandberg, W.F.; Whitworth, G.E.; Vocadlo, D.J.; Walker, S. Structural Snapshots of the Reaction Coordinate for O-GlcNAc Transferase. *Nat. Chem. Biol.* **2012**, *8*, 966–968, doi:10.1038/nchembio.1109.
- Konrad, R.J.; Zhang, F.; Hale, J.E.; Knierman, M.D.; Becker, G.W.; Kudlow, J.E. Alloxan Is an Inhibitor of the Enzyme O-Linked N-Acetylglucosamine Transferase. *Biochem. Biophys. Res. Commun.* **2002**, *293*, 207–212, doi:10.1016/S0006-291X(02)00200-0.
- Gloster, T.M.; Zandberg, W.F.; Heinonen, J.E.; Shen, D.L.; Deng, L.; Vocadlo, D.J. Hijacking a Biosynthetic Pathway Yields a Glycosyltransferase Inhibitor within Cells. *Nat. Chem. Biol.* **2011**, *7*, 174–181, doi:10.1038/nchembio.520.
- Gross, B.J.; Kraybill, B.C.; Walker, S. Discovery of O-GlcNAc Transferase Inhibitors. *J. Am. Chem. Soc.* **2005**, *127*, 14588–14589, doi:10.1021/ja0555217.
- Jiang, J.; Lazarus, M.B.; Pasquina, L.; Sliz, P.; Walker, S. A Neutral Diphosphate Mimic Crosslinks the Active Site of Human O-GlcNAc Transferase. *Nat. Chem. Biol.* **2012**, *8*, 72–77, doi:10.1038/nchembio.711.
- Martin, S.E.S.; Tan, Z.W.; Itkonen, H.M.; Duveau, D.Y.; Paulo, J.A.; Janetzko, J.; Boutz, P.L.; Törk, L.; Moss, F.A.; Thomas, C.J.; et al. Structure-Based Evolution of Low Nanomolar O-GlcNAc Transferase Inhibitors. *J. Am. Chem. Soc.* **2018**, *140*, 13542–13545, doi:10.1021/jacs.8b07328.
- Loi, E.M.; Weiss, M.; Pajk, S.; Gobec, M.; Tomasic, T.; Pieters, R.J.; Anderluh, M. Intracellular Hydrolysis of Small-Molecule O-Linked N-Acetylglucosamine Transferase Inhibitors Differs among Cells and Is Not Required for Its Inhibition. *Molecules* **2020**, *25*, doi:10.3390/molecules25153381.
- Roy, K.; Kar, S.; Das, R.N. *Understanding the Basics of QSAR for Applications in Pharmaceutical Sciences and Risk Assessment.*; 2015; ISBN 9780128015056.
- Zhang, H.; Tomašič, T.; Shi, J.; Weiss, M.; Ruijtenbeek, R.; Anderluh, M.; Pieters, R.J. Inhibition of: O -GlcNAc Transferase (OGT) by Peptidic Hybrids. *Medchemcomm* **2018**, *9*, 883–887, doi:10.1039/c8md00115d.
- WuXi-AppTech DELOpen Available online: <https://hits.wuxiapptec.com/delopen> (accessed on 4 February 2022).
- Khalid, M.; Mohammed, S.; Kalo, A. Synthesis of Weinreb

- and Their Derivatives (A-Review). *Orient. J. Chem.* **2020**, *36*, 206–219, doi:10.13005/ojc/360201.
26. Adams, J.; Anderson, E.C.; Blackham, E.E.; Chiu, Y.W.R.; Clarke, T.; Eccles, N.; Gill, L.A.; Haye, J.J.; Haywood, H.T.; Hoenig, C.R.; et al. Structure Activity Relationships of Av Integrin Antagonists for Pulmonary Fibrosis by Variation in Aryl Substituents. *ACS Med. Chem. Lett.* **2014**, *5*, 1207–1212, doi:10.1021/ml5002079.
27. Tan, C.Y.K.; Weaver, D.F. A One-Pot Synthesis of 3-Amino-3-Arylpropionic Acids. *ChemInform* **2003**, *34*, 7449–7461, doi:10.1002/chin.200306087.
28. Rodríguez-Mata, M.; García-Urdiales, E.; Gotor-Fernández, V.; Gotor, V. Stereoselective Chemoenzymatic Preparation of  $\beta$ -Amino Esters: Molecular Modelling Considerations in Lipase-Mediated Processes and Application to the Synthesis of (S)-Dapoxetine. *Adv. Synth. Catal.* **2010**, *352*, 395–406, doi:10.1002/adsc.200900676.
29. Fujima, Y.; Ikunaka, M.; Inoue, T.; Matsumoto, J. Synthesis of (S)-3-(N-Methylamino)-1-(2-Thienyl)Propan-1-ol: Revisiting Eli Lilly's Resolution-Racemization-Recycle Synthesis of Duloxetine for Its Robust Processes. *Org. Process Res. Dev.* **2006**, *10*, 905–913, doi:10.1021/op060118l.
30. Krieglstein, M.; Profous, D.; Lyčka, A.; Trávníček, Z.; Přebylka, A.; Volná, T.; Benická, S.; Cankař, P. Axially Chiral Trifluoromethylbenzimidazolylbenzoic Acid: A Chiral Derivatizing Agent for  $\alpha$ -Chiral Primary Amines and Secondary Alcohols to Determine the Absolute Configuration. *J. Org. Chem.* **2019**, *84*, 11911–11921, doi:10.1021/acs.joc.9b01770.
31. Alteen, M.G.; Gros, C.; Meek, R.W.; Cardoso, D.A.; Busmann, J.A.; Sangouard, G.; Deen, M.C.; Tan, H.Y.; Shen, D.L.; Russell, C.C.; et al. A Direct Fluorescent Activity Assay for Glycosyltransferases Enables Convenient High-Throughput Screening: Application to O-GlcNAc Transferase. *Angew. Chemie - Int. Ed.* **2020**, *59*, 9601–9609, doi:10.1002/anie.202000621.